15TH IEA HEAT PUMP CONFERENCE
MAY 26–29, 2026 | HOFBURG
VIENNA 2026
DECARBONISATION THROUGH INNOVATION

District Heating Integration for High-Temperature Heat Pumps: Assessing the Optimal Trade-Off between Environmental and Economic Benefits

Giovanna Pallotta[a*], Ghad Alarnaot-Alarnaout[b], Elisa Marrasso[a], Carlo Roselli[a], Joaquín Navarro-Esbrí[b], Adrian Mota-Babiloni[b]

[a]University of Sannio, P.zza Roma 21, Benevento 82100, Italy
[b]ISTENER Research Group, Department of Mechanical Engineering and Construction, Campus de Riu Sec, Castelló 12071, Spain

Abstract

This study presents a multi-objective optimization of a moderately high-temperature heat pump (HTHP) prototype using the low-global-warming-potential refrigerant R-450A, aiming to identify an optimal balance between energy performance and economic benefits. Building upon previous experimental work, empirical grey-box models derived from steady-state tests serve as the foundation for simulating the HTHP operation under various condensation temperatures (70, 80, 90, and 100 °C) and heat source conditions represented by different district heating networks. The optimization process utilizes a genetic algorithm to vary the evaporation temperature and compressor frequency, aiming to maximize both the coefficient of performance and the net hourly economic benefit. Results reveal a trade-off between these objectives: while higher evaporation temperatures generally improve both performance and hourly net cash-flows, reducing compressor frequency favors energy performance but can decrease profitability. The Pareto fronts derived illustrate that the real optimum operating points offer a balanced compromise, yielding significant cost savings without substantial losses in performance. An environmental assessment reveals that even under unfavorable high condensation temperatures, the real optimum point reduces carbon dioxide emissions for HTHP operation, emphasizing its environmental advantage. Conversely, maximizing economic gains slightly reduces environmental benefits, while maximizing the coefficient of performance alone is the least economically favorable solution. These findings underscore the importance of integrated optimization strategies that consider both economic and environmental dimensions in HTHP operation. The study also highlights the influence of regional electricity mix and energy market conditions on results, suggesting the need for tailored analyses in different contexts.

Keywords: Economic Profitability; Carbon Dioxide Emissions; High Temperature Heat Pump; Multi-objective Optimization.

1. Introduction

In 2024, the average global temperature exceeded 1.5 °C above pre-industrial levels for the first time. [1], underscoring the urgent need to accelerate greenhouse gas emission reductions in key high-emitting sectors. Industrial process heat accounts alone for approximately 18% of total global annual greenhouse gas emissions, equivalent to the combined emissions of the United States and India [2]. Despite the critical importance of decarbonizing this sector, the share of renewable energy used for industrial heat supply increased only modestly, from 10% to 12%, between 2015 and 2023 [3]. In this context, electrification turns out to be one of the most suitable solutions not only for low-temperature, but also medium- and high-temperature heat supply in industry [4] and high-temperature heat pumps (HTHPs) are expected to play a crucial role in the long-term decarbonization strategy of the industrial sector [5].

1.1. Background and literature review

While heat pumps are already well-established for domestic heating and cooling, there remains significant potential for technological advancements in high-temperature industrial applications [6]. Numerous scientific studies investigate ways to improve energy efficiency by combining HTHPs with thermal energy storage systems [7], utilizing waste heat [8], or integrating them with renewable energy sources [9] under various working conditions. The performance of HTHPs is typically evaluated based on the refrigerant used [10], the working configuration [11], and temperature levels [12], also adopting multi-purpose optimization techniques. Branchini et al. [13] employ a multi-purpose approach that combines thermodynamic modeling with the selection of design parameters to assess the adoption of HTHPs in the ceramic tile industry, incorporating innovative waste heat recovery systems. Dong et al. [14] propose a bi-level programming model based on a Getser-inspired algorithm. In the first level, the performance of HTHP under various working conditions is evaluated. In the second level, different system configurations are generated and ranked using an improved non-dominated sorting genetic algorithm. Li et al. [15] apply an optimization method to a trans-critical HTHP with CO_2 to address the phase equilibrium challenges introduced by the ejector. In the work by Vannoni et al. [16], the techno-economic performance of large-scale vapor compression systems is analyzed and optimized, considering the type of working fluid, source and supply temperatures, and addressing the significant knowledge gap related to their interdependence. The optimization process carried out by Xu et al. [17] aims to select the most suitable working fluid for the operation of HTHPs in various configurations. It employs the Non-dominated Sorting Genetic Algorithm II (NSGA-II) algorithm, using the COP and volumetric heating capacity as objective functions.

Optimizing the working conditions of HTHPs typically involves trade-offs between potentially conflicting requirements [18]. High electricity prices relative to natural gas are often identified as one of the main barriers to the widespread adoption of heat pumps for industrial heat supply in place of traditional boilers [19]. Jesper et al. [20] highlight that the interest rate, natural gas price, and electricity price all significantly affect the economic performance of heat pumps in industrial applications. The competitiveness of HTHPs in industrial applications is also evaluated in the study by Obrist et al. [21], which demonstrates that implementing seasonal flexibility is essential for optimal operation and for mitigating the impact of rising electricity prices during winter and spring. Cortvriendt et al. [22] consider a fixed carbon tax of 150 €/tCO_2 in the comparison of a heat pump system, an electric heater, and a natural gas boiler. The economic analysis conducted by Ma et al. [23] on an HTHP designed for steam supply considers not only the revenue from steam sales but also the economic benefits of industrial waste heat recovery in calculating the annual net profit. Sadeghi et al. [24] demonstrate the cost-effectiveness of an HTHP integrated with district heating networks (DHNs) as heat sources compared to electric or natural gas boilers. However, the cost-effectiveness of the proposed solution can increase significantly when free heat sources, such as air or waste heat, replace the DHN. In a previous publication [25], the authors analyzed a moderately HTHP prototype using R-450A and compared it with a conventional natural gas-fired boiler. A simulation-based approach is adopted, in which the HTHP is assumed to interact with various generations of DHN. The results demonstrate that the temperature lift significantly influences the performance of the HTHP, making its interaction with low-temperature DHNs or district cooling networks less favorable from both energy and environmental perspectives. Conversely, HTHP achieves economic savings over the conventional boiler only in configurations where heat is not purchased from the DHNs, that is, scenarios that are nonetheless less advantageous in terms of energy performance and environmental impact.

1.2. Aim of the paper

This paper builds on the main findings of the literature review and deepens the analysis conducted by the authors in a previous work [25]. This research aims to revisit the previous results and identify an optimal trade-off between the energy, environmental, and economic benefits of a moderately HTHP prototype using R-450A and interacting with various generation DHNs. In doing so, the study contributes to a broader scientific effort that addresses the variability of HTHP operating conditions for assessing their advantages over conventional systems. At the same time, it expands the analytical scope by applying a unified optimisation framework that balances energy and economic objectives, thereby moving beyond a focus solely on energy performance and environmental impact.

2. Methods

2.1. Experimental equipment

The single-stage vapor compression system with the liquid-to-suction heat exchanger (LSHX) investigated in this study is shown in Figure 1. It includes a semi-hermetic compressor (maximum power input of 7.6 kW, displacement of 22.7 m³/h, 1450 rpm at 50 Hz) equipped with a frequency inverter. The evaporator and the LSHX are both brazed plate heat exchangers, whereas the condenser is a finned-tube heat exchanger. The system incorporates an electronic expansion valve with a bypass that regulates valve opening, thereby controlling the activation of the LSHX. Additional components include a liquid receiver, oil separator, filter drier, sight glass, and various safety devices. The heat source is simulated by a secondary closed-loop circuit containing ethylene glycol and an 80 L buffer tank. Three electric resistances are installed in this loop, with a total heating capacity of 14.6 kW. A proportional-integral-derivative (PID) controller regulates one of the resistances by monitoring and adjusting the evaporation temperature. PID controllers manage the fan frequency inverter to regulate the condensation temperature, too, as well as the electronic expansion valve. A personal computer collects all measured data at one-second intervals, with a data acquisition system enabling real-time visualization. Steady-state conditions are considered achieved when both condensation and evaporation temperatures stabilize within a ±1 K range. Under these conditions, data recording begins and continues for 20 minutes. Final steady-state results are obtained by averaging the raw measurement data over this period. Additional thermodynamic steady-state properties are estimated using REFPROP v10.0 [26]. As anticipated, the refrigerant used in the experimental tests is R-450A, a non-flammable, low-toxicity mixture of the hydrofluorocarbon R-134a and the hydrofluoroolefin R-1234ze(E), with a global warming potential (GWP) of 547.

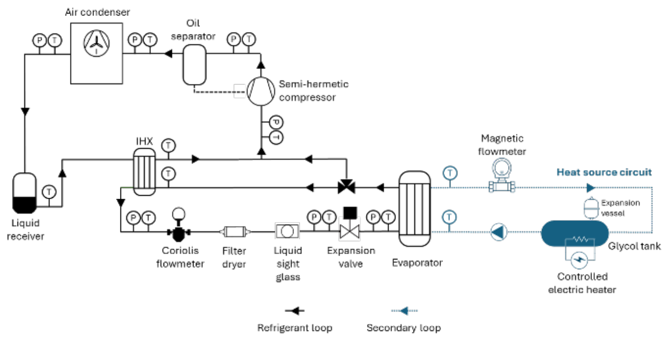

Figure 1. Layout of the experimental rig.

The wide range of conditions reproduced with the LSHX OFF is summarised in Table 1, where T^{EVAP}, T^{COND}, f^{COMP}, PR, COP and $\dot{Q}_{th}^{COND}$ represent the evaporation temperature, condensation temperature, compressor frequency, pressure ratio, coefficient of performance, and condenser load, respectively. T^{EVAP} varies between 2 and 40 °C, while T^{COND} ranges from 45 to 85 °C. Figure 2 shows the P-h and T-s diagrams for conditions with the minimum and maximum PR, which are 30-65 °C and 2-65 °C, respectively.

Table 1. Operating conditions tested.

T^{EVAP} [°C]	T^{COND} [°C]	f^{COMP} [Hz]	PR [-]	COP [-]	$\dot{Q}_{th}^{COND}$ [-]
19.7	65.2	35.0	3.5	4.2	14.7
29.4	65.2	35.0	2.6	4.7	17.6
39.6	79.8	35.0	2.7	3.6	19.0
40.3	84.9	35.0	2.9	3.0	17.5
2.4	45.2	40.0	3.9	3.9	10.3
9.4	55.5	40.0	3.9	3.9	12.6
10.4	65.2	40.0	4.7	3.2	11.6

9.8	74.8	40.0	5.9	2.6	10.1
19.6	79.7	40.0	4.8	2.7	12.6
29.8	79.7	45.0	3.6	3.2	17.4
34.6	84.9	40.0	3.5	2.9	17.7
1.8	55.5	45.0	5.1	3.2	10.5
1.3	65.2	45.0	6.4	2.6	9.3
9.8	79.7	50.0	6.6	2.4	12.5

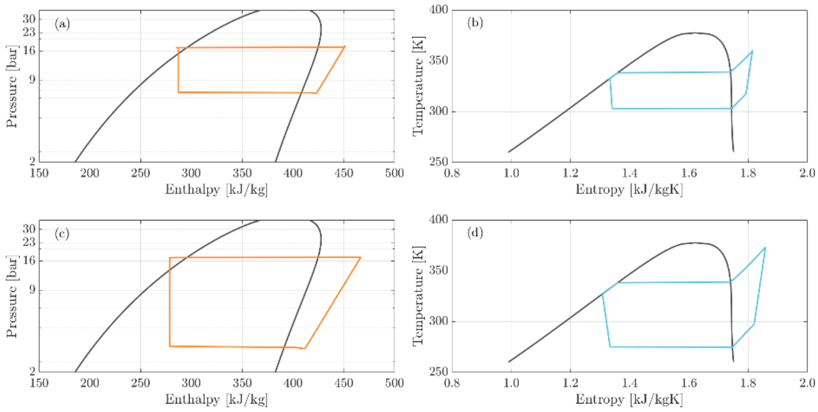

Figure 2. P-h diagram for the condition 30–65 °C (a). T-s diagram for the condition 30–65 °C (b). P-h diagram for the condition 2–65 °C (c). T-s diagram for the condition 2–65 °C (d).

2.2. Simulation models

The results of the experimental tests with the LSHX turned off served as the basis for developing grey-box empirical models of the HTHP. These models were constructed using multivariable linear regression analysis applied to the experimental data [25]. The corresponding model coefficients, presented in Table 2 and applied in Eq. (1), are used in this study within a simulation-based optimisation framework. The aim is to balance two conflicting objectives: improving the energy performance and maximising the economic benefits of the moderately-HTHP supplying thermal energy at different temperatures and operating with various heat sources, namely different generation DHNs. Specifically, Eq. (1) has been used to estimate f^{COMP}, $\dot{Q}_{out}^{COND}$, and PR as functions of T^{EVAP}, T^{COND} and f^{COMP}. In particular, T^{EVAP} and f^{COMP} are the decision variables in the optimisation process, as detailed in the following section.

Table 2. Coefficients of the linear multi-variable empirical models built using experimental data.

Function	a	b	c	d
COP [-]	0.0467	-0.0663	-0.0168	7.7584
PR [-]	-0.1288	0.0965	0.0109	-0.5335
$\dot{Q}_{th}^{COND}$ [kW]	0.3437	-0.1147	0.2122	6.9521

$$y = a \cdot T^{EVAP} + b \cdot T^{COND} + c \cdot f^{COMP} + d \quad (1)$$

2.3. Multi-objective optimization

The multi-objective optimisation conducted in this study is implemented in MATLAB [27] using the *gamultiobj* function. This function utilizes a controlled elitist genetic algorithm, a variant of the NSGA-II. This method can handle multiple conflicting objectives and is suitable for complex or nonlinear problems. It supports variable bounds and constraints, and produces a set of Pareto-optimal solutions, showing the trade-offs between objectives. Furthermore, its flexibility and reliability make it well-suited for real-world optimization problems. The input parameters include the objective functions, the number of decision variables, non-linear and linear constraints, and the lower and upper bounds for each decision variable.

As previously mentioned, the decision variables are T^{EVAP} and f^{COMP}, which are allowed to vary within 30 and 50 °C and 35 and 50 Hz, respectively. It is important to note that varying T^{EVAP} corresponds to changing the heat source interacting with the HTHP. The selected temperature levels may be representative of different types of DHNs. However, in this study, no further details regarding the heat source are specified beyond the temperature level, as the primary aim of the analysis is to conduct a theoretical assessment based on variations in source temperature. In this context, DHNs are considered a potential application due to the different temperature levels characterizing their various generations. In contrast, T^{COND} is fixed at four discrete values to represent various working conditions for different intended applications. The values chosen for T^{COND} are 70, 80, 90, and 100 °C, respectively. The optimisation process is repeated for each T^{COND}, with the primary aim of determining the optimal T^{EVAP} and f^{COMP} that maximize the two conflicting objective functions.

The adopted objective functions encompass both energy and economic perspectives, with the former indirectly contributing to environmental benefits:

- the energy-related objective is the COP, calculated as defined in Eq. (1), considering the coefficients indicated in Table 2.
- The economic objective function is the hourly net cash-flow (C_{net}) associated with operating the HTHP, as defined in Eq. (2). C_{net} is determined by subtracting the expenditures for thermal energy purchased from the heat source DHN ($\dot{Q}_{th}^{EVAP}$) and the electricity requested by the HTHP compressor ($\dot{L}_{el}^{COMP}$), to the revenue generated from selling thermal energy. In Eq. (2), $\dot{Q}_{th}^{COND}$ is calculated using Eq. (1) and the coefficients listed in Table 2; $\dot{L}_{el}^{COMP}$ is determined as the ratio of $\dot{Q}_{th}^{COND}$ to the COP; and $\dot{Q}_{th}^{EVAP}$ is quantified according to Eq. (3). The unit price of DHN-supplied heat (p_{th}^{DHN}) is assumed to be 80 €/MWh [28], while the heat produced and sold by the HTHP is assumed to have a unit price (p_{th}^{HTHP}) of 140 €/MWh [28]. The electricity price (p_{el}) is set to 166 €/MWh, based on the average cost of electricity in Europe for non-household consumers in the period from 2011 to 2024 [29].

Lastly, a non-linear constraint related the PR is applied in the optimisation process. The PR is calculated using Eq. (1) and the coefficient listed in Table 2, ensuring that the optimization results remain consistent with the thermodynamic limitations of the system.

$$C_{net} = \dot{Q}_{th}^{COND} \cdot p_{th}^{HTHP} - \dot{L}_{el}^{COMP} \cdot p_{el} - \dot{Q}_{th}^{EVAP} \cdot p_{th}^{DHN} \tag{2}$$

$$\dot{Q}_{th}^{EVAP} = \dot{Q}_{th}^{COND} - \dot{L}_{el}^{COMP} \tag{3}$$

3. Results and Discussion

Figure 3 shows the trend of the COP as T^{EVAP} and f^{COMP} vary, with T^{COND} held constant. In the first, second, third, and fourth graphs, T^{COND} is 70, 80, 90, and 100 °C, respectively. It is observed that as T^{COND} increases, the COP decreases. In fact, when T^{COND} is 70 °C, the maximum and minimum COP values are 5.0 and 3.0, respectively. These values are significantly higher than those obtained at a condensation temperature of 100 °C, which are 3.0 and 1.5, respectively. Nevertheless, the trend of the COP with respect to the considered variables remains the same, regardless of the condensation temperature, and increases with rising T^{EVAP} and decreasing f^{COMP}.

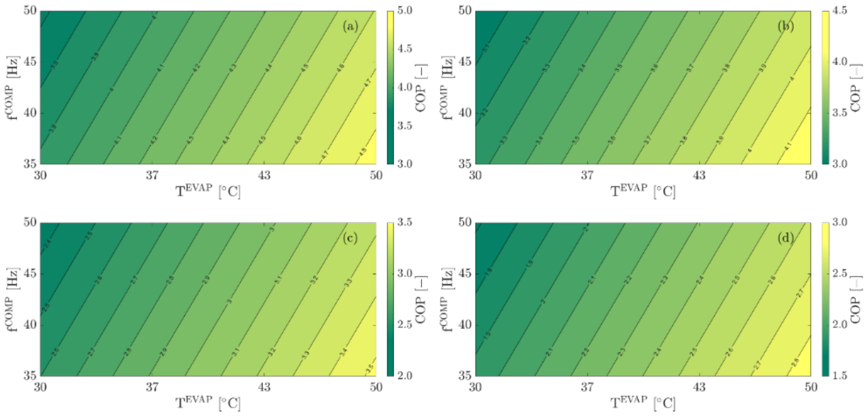

Figure 3. Trend of the COP with evaporation temperature and compressor frequency at condensation temperatures of 70 °C (a), 80 °C (b), 90 °C (c) and 100 °C (d).

Figure 4 shows the trend of C_{net} as a function of T^{EVAP} and f^{COMP}, with the T^{COND} held constant. The goal is to maximize C_{net} as defined (the difference between the revenue from the sale of thermal energy and the total expenses). The results obtained are partially in contrast to those related to the COP. In fact, increasing T^{COND} generally leads to a reduction in C_{net}, and the trend is such that the C_{net} increases with increasing T^{EVAP}, consistently with what was observed for the COP. However, unlike the COP, C_{net} decreases as f^{COMP} decreases in most cases. For instance, when T^{COND} equals 70°C, the maximum C_{net} of approximately 1.1 EUR/h is found at a T^{EVAP} and f^{COMP} of 50°C and 50 Hz, respectively. In this condition, the COP equals 4.6 and is slightly lower than the value found at minimum f^{COMP} but the same T^{EVAP}. Hence, maximizing the COP (and the resulting energy and environmental benefits) could lead to a reduction in the system's profit. The objective is to estimate the extent to which these goals conflict by determining the optimal operating conditions for the HTHP.

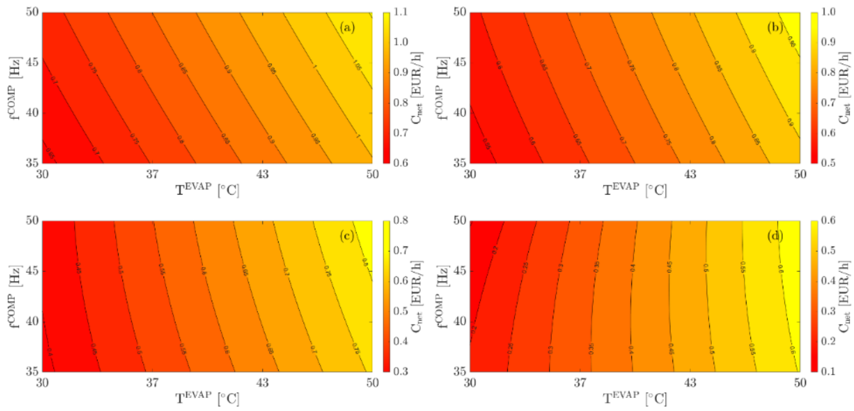

Figure 4. Trend of the hourly net cash flows with evaporation temperature and compressor frequency at condensation temperatures of 70 °C (a), 80 °C (b), 90 °C (c) and 100 °C (d).

Figure 6 shows the trend of the Pareto front obtained from the optimization process by adjusting the decision variables (T^{EVAP} and f^{COMP}), with the T^{COND} fixed (at 70, 80, 90, and 100 °C as in the previous cases). For each T^{COND}, a variation in the COP of about 0.2 is observed along the Pareto front. For example, in the case with T^{COND} at 70 °C, the Pareto front covers COP values ranging from approximately 4.38 to 4.55. In the case with T^{COND} at 100 °C, the COP along the Pareto front ranges from about 2.63 to 2.87. On the other hand, the variability of C_{net} tends to be less pronounced as T^{COND} increases. For instance, with T^{COND} at 70 °C, C_{net} varies from approximately 0.87 to about 0.99 €/h; in the case with T^{COND} at 100 °C, C_{net} ranges instead from about 0.60 to around 0.63 €/h.

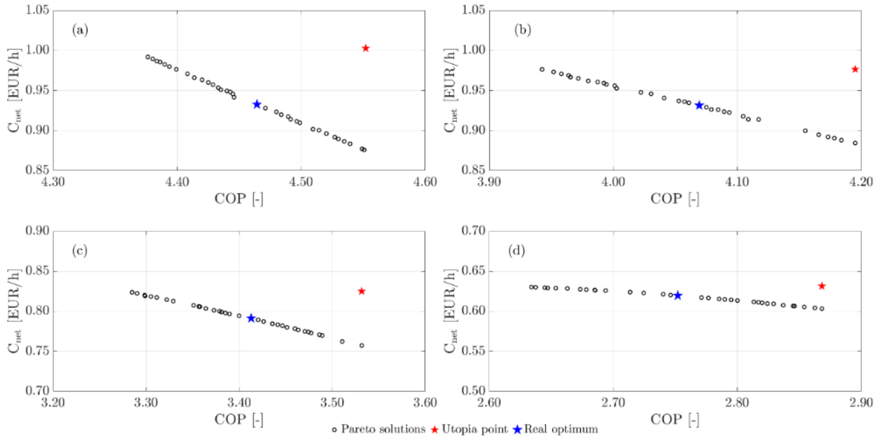

Figure 5. Pareto front at condensation temperatures of 70 °C (a), 80 °C (b), 90 °C (c) and 100 °C (d).

Despite the limited variability of the results obtained on the Pareto front, it is interesting to compare the non-dominated solutions with all the solutions calculated during the execution of the genetic algorithm, as shown in Figure 6. In the graphs presented (each corresponding to a specific T^{COND}, from 70 to 100 °C), the trend of the results for each generation within the algorithm is shown. Starting from relatively low COP and C_{net} values, as the generations progress, the solutions converge toward increasingly higher values, where the Pareto front is also located. The COP rises by approximately, at least, 0.5. For example, in the case with T^{COND} at 70 °C, the COP increases from about 3.9 to about 4.6; with T^{COND} at 100 °C, the COP increases from about 2.2 to about 2.9.

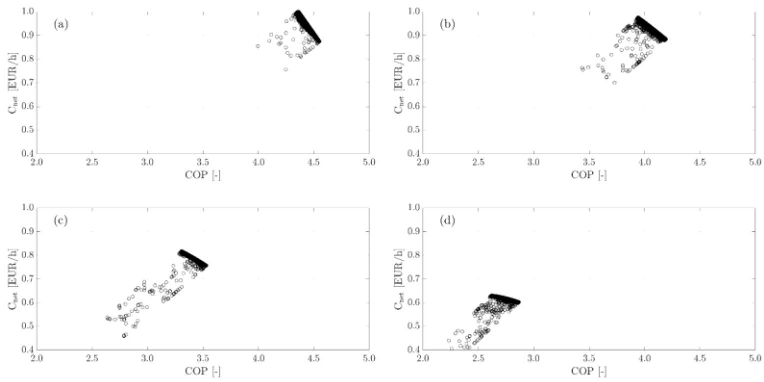

Figure 6. Solutions explored by executing the genetic algorithm at condensation temperatures of 70 °C (a), 80 °C (b), 90 °C (c) and 100 °C (d).

Figure 7 shows the set of all explored decision variable values. Although the solutions exhibit some variability in the initial iterations, as the algorithm progresses, the decision variable values cluster around the values of high evaporation temperatures, showing variability only with respect to the compressor frequency. The actual optimal values of the decision variables, compared with the ideal optimal values, are reported for each condensation temperature in Table 3.

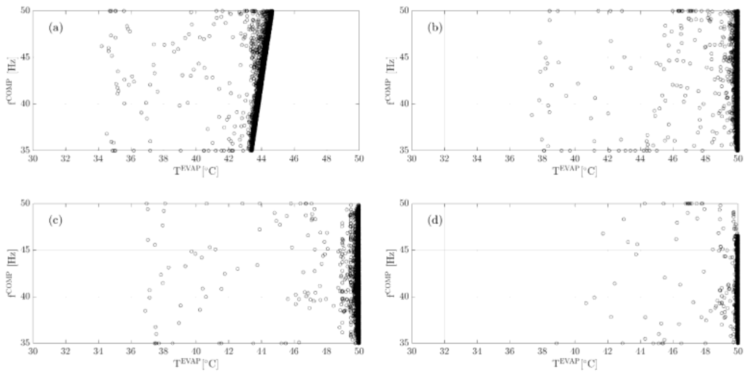

Figure 7. Set of explored decision variables at condensation temperatures of 70 °C (a), 80 °C (b), 90 °C (c) and 100 °C (d).

Table 3. Values of the decision variables at the real optimum, maximum coefficient of performance, and maximum net cash flow.

T^{COND} [°C]	Real optimum solution		Solution with maximum COP		Solution with maximum C_{net}	
	T^{EVAP} [°C]	f^{COMP} [Hz]	T^{EVAP} [°C]	f^{COMP} [Hz]	T^{EVAP} [°C]	f^{COMP} [Hz]
70	44.08	42.78	43.43	35.00	44.71	50.00
80	49.98	42.69	50.00	35.00	50.00	50.00
90	49.99	42.36	50.00	35.00	50.00	50.00
100	49.99	41.33	50.00	35.00	50.00	50.00

The results obtained in the real optimum point can be compared with those corresponding to the maximum COP and maximum C_{net}. In this framework, the energy objective is translated into an environmental-one, by analyzing the equivalent carbon dioxide (CO_2) emissions associated with HTHP operation. Equivalent CO_2 emissions are calculated using the average CO_2 power grid emission factor for the Italian electricity mix in 2022, which is 0.286 $kgCO_2/kWh_{el}$ [30]. Figure 8 shows the values of equivalent CO_2 emissions and C_{net} relative to the solutions with maximum COP, maximum C_{net}, and real optimum, for each T^{COND}. As previously mentioned, increasing T^{COND} reduces both the energy performance (i.e., environmental advantages) and the economic benefits. From an economic perspective, operating under maximum COP conditions turns out to be the most disadvantageous solution. If the real optimum condition is preferred with T^{COND} at 70 °C, the C_{net} increases from 0.87 to 0.94 EUR/h. Assuming the HTHP operates continuously throughout the year, except for one week of scheduled maintenance, the additional hourly profit of 0.07 EUR/h corresponds to approximately 601 EUR in annual additional earnings. On the other hand, maximizing the C_{net} leads to a reduction in performance, resulting in diminished environmental benefits. The most notable case occurs at a T^{COND} of 100 °C. Indeed, operating under real optimum conditions reduces CO_2 emissions to approximately 2.3 $kgCO_2/h$, thereby improving environmental performance even within an already particularly unfavorable operating scenario.

In conclusion, the comparison between the real optimum operating point and the solutions with maximum COP or C_{net} highlights the necessary trade-offs between economic and environmental objectives. The results demonstrate that the choice of operating strategy has a significant impact on both cost-effectiveness and CO_2 emissions. Although the differences may appear marginal on an hourly basis, their cumulative effect over time is substantial. Overall, these findings indicate that a system-level optimization approach, rather than focusing solely on COP or C_{net}, can lead to more sustainable and economically viable HTHP operation. The real optimum point not only increases long-term profit but also enhances environmental performance, particularly in challenging high-temperature scenarios. However, the results of the environmental analysis are closely linked to the Italian electricity production mix in 2022. Different CO_2 emission factors for the power grid, as observed in countries with different electricity generation mixes, would lead to different environmental outcomes. Similarly, economic optimization is influenced by local market conditions that govern the purchase and sale of thermal and electric energy. Under different regulatory or pricing regimes, the optimal balance between COP (i.e., environmental impact) and C_{net} may shift considerably.

Building upon the findings of this study, several potential directions for future research emerge. Firstly, incorporating dynamic electricity pricing models into the optimization framework would provide a more realistic assessment of economic performance. Indeed, considering real-time tariffs could reveal how variations in energy prices impact the optimal operating conditions and overall revenues. Secondly, extending the analysis to include multiple countries with different power grid emission factors and market conditions would improve the generalizability of the results. This would enable the assessment of the environmental and economic benefits of HTHPs across diverse regulatory and energy landscapes.

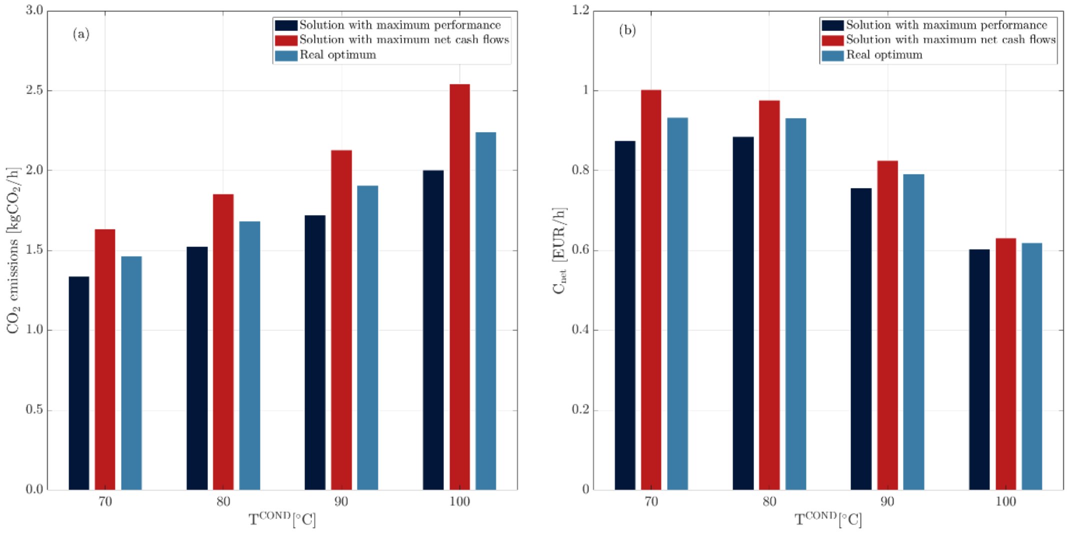

Figure 8. Hourly equivalent carbon dioxide emissions (a) and net cash-flows (b).

4. Conclusions

This study revisits and extends previous work on a moderately high-temperature heat pump prototype using R-450A, applying a multi-objective optimization framework to balance energy performance and economic benefits. The analysis considered various condensation temperatures and different generation district heating networks as heat sources, with decision variables including evaporation temperature and compressor frequency.

Results demonstrate a clear trade-off between maximizing the coefficient of performance and achieving the highest net economic benefit. While increasing the evaporation temperature generally improves the coefficient of performance and net cash flows, reducing the compressor frequency favors the coefficient of performance but can reduce economic gains. The Pareto optimization reveals that operating at the real optimum, a compromise between energy performance and costs, yields substantial economic savings with minimal degradation in performance. Subsequent environmental analysis reveals that the optimal operation point achieves lower carbon dioxide emissions, particularly at higher condensation temperatures, where system operation is more challenging. Although maximizing the net cash flow slightly diminishes environmental benefits, operating solely to optimize performance results in the least favorable economic outcome.

The study underscores the importance of adopting a system-level optimization approach rather than focusing solely on either energy performance or economic profitability. It also emphasizes that results depend strongly on regional electricity emission factors and local market conditions, which affect both environmental and financial outcomes. Future research should explore the incorporation of dynamic electricity pricing and expand the analysis to different geographic and regulatory contexts to enhance the applicability and robustness of the optimization framework.

Acknowledgements

The authors acknowledge the project Sharing Heat and Knowledge on Energy Communities (SHaKE). > Grant No. 2023-1-HU01-KA220-HED-000160219, funded by Erasmus+, and the project LEO23-2-9632-ING-ING-4 funded by Fundación BBVA.

Nomenclature

Acronyms and abbreviations

CO_2	Carbon Dioxide
DHN	District Heating Network
GWP	Global Warming Potential
HTHP	High Temperature Heat Pump
LSHX	Liquid-to-Suction Heat Exchanger
NSGA-II	Non-dominated Sorting Genetic Algorithm II
PID	Proportional Integrative Derivative

Symbols

C_{net}	Net hourly cash-flow [EUR/h]
COP	Coefficient Of Performance [-]
f^{COMP}	Compressor frequency [Hz]
$\dot{L}_{el}^{COMP}$	Compressor power [kW]
$\dot{Q}_{th}^{COND}$	Condenser heat load [kW]
$\dot{Q}_{th}^{EVAP}$	Haet absorbed by the evaporator [kW]
p_{el}	Electricity price [EUR/MWh]
p_{th}^{DHN}	Thermal energy price [EUR/MWh]
p_{th}^{HTHP}	Thermal energy selling price [EUR/MWh]
PR	Pressure Ratio [-]
T^{COND}	Condensation temperature [°C]
T^{EVAP}	Evaporation temperature [°C]

References

[1] Copernicus, “Copernicus: 2024 is the first year to exceed 1.5°C above pre-industrial level.” Accessed: Jul. 17, 2025. [Online]. Available: Copernicus: 2024 is the first year to exceed 1.5°C above the pre-industrial level

[2] World Business Council for Sustainable Development, “Industrial heat: an overlooked piece in the decarbonization puzzle.” Accessed: Jul. 17, 2025. [Online]. Available: https://www.wbcsd.org/news/industrial-heat-an-overlooked-piece-in-the-decarbonization-puzzle/

[3] International Energy Agency, “Renewables 2023,” Paris, 2024. Accessed: Jul. 17, 2025. [Online]. Available: https://www.iea.org/reports/renewables-2023.

[4] L. M. Pastore *et al.*, “Long-term decarbonisation of hard-to-abate industrial thermal demand for 100 % renewable energy systems,” *Energy*, vol. 327, p. 136384, Jul. 2025, doi: 10.1016/j.energy.2025.136384.

[5] Technology Collaboration Programme on Heat Pumping Technologies, “Annex 58. High -Temperature Heat Pumps. Task 3 – Applications and Transition,” Borås, 2024. doi: 10.23697/dn21-0b02.

[6] J. Gollasch, M. Kriese, J. Siegel, N. Kabat, and J. Walden, “Numerical investigation of a heat pump demonstrator for partial electrification of the steam supply for paper drying,” *Appl Therm Eng*, vol. 278, p. 126941, Nov. 2025, doi: 10.1016/j.applthermaleng.2025.126941.

[7] A. Passamonti, F. Sachse, P. Bombarda, and R. Bracke, “Design, construction, and commissioning of a 500 kW high-temperature heat pump plant for the district heating network of Bochum, Germany,” *Energy Reports*, vol. 13, pp. 548–561, Jun. 2025, doi: 10.1016/j.egyr.2024.11.080.

[8] X. Shi, C. Zhang, Y. Liu, and F. Wang, “Investigation on multi-stage compression high-temperature heat pump system based on R718 and other low GWP refrigerants,” *International Journal of Refrigeration*, vol. 176, pp. 238–253, Aug. 2025, doi: 10.1016/j.ijrefrig.2025.04.019.

[9] Z. Claudio and F. Daniele, “High-temperature heat pumps for geothermal applications in Africa: thermodynamic, economic and environmental evaluation,” *Appl Therm Eng*, vol. 278, p. 127302, Nov. 2025, doi: 10.1016/j.applthermaleng.2025.127302.

[10] Z. Hao, A. Wu, Z. Zhang, J. Hua, Y. Lin, and D. Cai, “Comprehensive assessment of high-temperature heat pumps using novel low-GWP refrigerant mixtures as working fluids: Energy, exergy, thermal properties, and safety,” *Thermal Science and Engineering Progress*, vol. 64, p. 103786, Aug. 2025, doi: 10.1016/j.tsep.2025.103786.

[11] E. Vieren, T. Demeester, W. Beyne, A. Arteconi, M. De Paepe, and S. Lecompte, “The thermodynamic potential of high-temperature transcritical heat pump cycles for industrial processes with large temperature glides,” *Appl Therm Eng*, vol. 234, p. 121197, Nov. 2023, doi: 10.1016/j.applthermaleng.2023.121197.

[12] J. Famiglietti, L. Acconito, C. Arpagaus, and T. Toppi, “Environmental life cycle assessment of industrial high-temperature to residential small-size heat Pumps: A critical review,” *Energy Conversion and Management: X*, vol. 26, p. 100947, Apr. 2025, doi: 10.1016/j.ecmx.2025.100947.

[13] L. Branchini, A. De Pascale, S. Ottaviano, and C. Poletto, “Application of high-temperature heat pumps in the ceramic tiles manufacturing sector for waste heat harnessing,” *Appl Therm Eng*, vol. 274, p. 126694, Sep. 2025, doi:

10.1016/j.applthermaleng.2025.126694.
[14] S. Dong, P. Hu, C. Zhang, X. Hu, W. Zhuang, and D. Wu, "How to optimally design industrial high-temperature heat pump for multiple objectives and working conditions?," *Energy*, vol. 329, p. 136830, Aug. 2025, doi: 10.1016/j.energy.2025.136830.
[15] W. Li, B. Yue, H. Zhang, C. Zheng, P. Jiang, and Y. Zhu, "Optimization of trans-critical CO2 high-temperature heat pump cycle and study of maximum heating temperature," *International Journal of Refrigeration*, vol. 177, pp. 99–110, Sep. 2025, doi: 10.1016/j.ijrefrig.2025.05.023.
[16] A. Vannoni, A. Sorce, A. Traverso, and A. Fausto Massardo, "Large size heat pumps advanced cost functions introducing the impact of design COP on capital costs," *Energy*, vol. 284, p. 129204, Dec. 2023, doi: 10.1016/j.energy.2023.129204.
[17] C. Xu, H. Ma, and X. Yu, "Comprehensive performance evaluation method of working fluids for high temperature heat pump based on multi-objective optimization," *Appl Therm Eng*, vol. 247, p. 123102, Jun. 2024, doi: 10.1016/j.applthermaleng.2024.123102.
[18] A. Fernández-Moreno, A. Mota-Babiloni, P. Giménez-Prades, and J. Navarro-Esbrí, "Optimal refrigerant mixture in single-stage high-temperature heat pumps based on a multiparameter evaluation," *Sustainable Energy Technologies and Assessments*, vol. 52, p. 101989, Aug. 2022, doi: 10.1016/j.seta.2022.101989.
[19] C. A. McMillan and L. Wachs, "Industrial process heat decarbonization: A user-centric perspective," *Energy Res Soc Sci*, vol. 112, p. 103505, Jun. 2024, doi: 10.1016/j.erss.2024.103505.
[20] M. Jesper, F. Pag, K. Vajen, and U. Jordan, "Hybrid solar thermal and heat pump systems in industry: Model based development of globally applicable design guidelines," *Solar Energy Advances*, vol. 3, p. 100034, 2023, doi: 10.1016/j.seja.2023.100034.
[21] M. D. Obrist, R. Kannan, R. McKenna, T. J. Schmidt, and T. Kober, "High-temperature heat pumps in climate pathways for selected industry sectors in Switzerland," *Energy Policy*, vol. 173, p. 113383, Feb. 2023, doi: 10.1016/j.enpol.2022.113383.
[22] L. Cortvriendt, D. Flórez-Orrego, D. Bongartz, and F. Maréchal, "Data-driven systematic methodology for predicting optimal heat pump integration based on temperature levels and refrigerants," *Energy Convers Manag*, vol. 326, p. 119495, Feb. 2025, doi: 10.1016/j.enconman.2025.119495.
[23] X. Ma, Y. Du, B. Lei, and Y. Wu, "Energy, exergy, economic, and environmental analysis of a high-temperature heat pump steam system," *International Journal of Refrigeration*, vol. 160, pp. 423–436, Apr. 2024, doi: 10.1016/j.ijrefrig.2024.01.020.
[24] M. Sadeghi, T. Petersen, Z. Yang, B. Zühlsdorf, and K. S. Madsen, "Thermal design and optimization of high-temperature heat pump integrated with district heating benchmarked in Denmark for process heat supply," *International Journal of Refrigeration*, vol. 159, pp. 356–370, Mar. 2024, doi: 10.1016/j.ijrefrig.2023.12.025.
[25] G. Pallotta, G. Alarnaot-Alarnaout, E. Marrasso, M. Sasso, J. Navarro-Esbrí, and A. Mota-Babiloni, "Techno-economic and environmental assessment of a moderately high-temperature heat pump prototype using R-450A across diverse operational conditions and heat sources," *Energy*, vol. 326, p. 136008, Jul. 2025, doi: 10.1016/j.energy.2025.136008.
[26] E. W. Lemmon, I. H. Bell, M. L. Huber, and M. O. McLinden, "NIST standard reference database 23: reference fluid thermodynamic and transport Properties-REFPROP, version 10.0," 2018. Accessed: Oct. 01, 2025. [Online]. Available: https://doi.org/10.18434/T4JS3C.
[27] Inc. The MathWorks, "MATLAB," 2023. Accessed: Oct. 22, 2025. [Online]. Available: https://it.mathworks.com/products/matlab.html.
[28] G. Alarnaot-Alarnaout, J. Navarro-Esbrí, Á. Barragán-Cervera, and A. Mota-Babiloni, "Energy, exergy, economic, and environmental (4E) assessment of an experimental moderately-high-temperature heat pump for district heating and cooling networks," *Energy Convers Manag*, vol. 325, p. 119346, Feb. 2025, doi: 10.1016/j.enconman.2024.119346.
[29] Eurostat, "Electricity price statistics – Data sources." Accessed: Oct. 22, 2025. [Online]. Available: https://ec.europa.eu/eurostat/statistics-explained/index.php?title=Electricity_price_statistics#Data_sources.
[30] E. Marrasso, C. Martone, G. Pallotta, C. Roselli, and M. Sasso, "Assessment of energy systems configurations in mixed-use Positive Energy Districts through novel indicators for energy and environmental analysis," *Appl Energy*, vol. 368, p. 123374, Aug. 2024, doi: 10.1016/j.apenergy.2024.123374.